Upconversion properties and temperature sensing behaviors in visible and near-infrared region based on fluorescence intensity ratio in LuVO$_4$: Yb^{3+}/Er^{3+}

Yan Ma [a], Guotao Xiang [a, *], Jiahua Zhang [b], Zhen Liu [a], Pan Zhou [a], Wen Liu [b, c], Xiao Tang [a], Sha Jiang [a], Xianju Zhou [a], Li Li [a], Yongshi Luo [b], Ye Jin [d]

[a] Department of Mathematics and Physics, Chongqing University of Posts and Telecommunications, 2 Chongwen Road, Chongqing 400065, China
[b] State Key Laboratory of Luminescence and Applications, Changchun Institute of Optics, Fine Mechanics and Physics, Chinese Academy of Sciences, 3888 Eastern South Lake Road, Changchun 130033, China
[c] Graduate School of Chinese Academy of Sciences, Beijing 100039, China
[d] School of Science, Chongqing University of Technology, 69 Hongguang Street, Chongqing 400054, China

ARTICLE INFO

ABSTRACT

A high temperature solid state method was used to synthesize the Yb^{3+} and Er^{3+} codoped LuVO$_4$. The efficient energy transfer (ET) processes from Yb^{3+} to Er^{3+} has been demonstrated by upconversion (UC) spectra, near-infrared (NIR) spectra and lifetime curves. The optimal doping concentration for Yb^{3+} and Er^{3+} is 20 mol % and 2 mol %, respectively. Meanwhile, the temperature sensing behaviors in visible and NIR region based on fluorescence intensity ratio (FIR) have been explored in detail. In visible region, the optical thermometry of LuVO$_4$: Yb^{3+}/Er^{3+} is investigated via the FIR of the two thermally coupled energy levels ^{2}H$_{11/2}$ and ^{4}S$_{3/2}$ of Er^{3+}, accompanying with a maximal absolute sensitivity S_A of 0.82% K^{-1} at 423 K. In NIR region, the FIRs of Peak 1 (located at 1595 nm) to Peak 3 (located at 1660 nm) and Peak 2 (located at 1637 nm) to Peak 3, which are all assigned to ^{4}I$_{13/2} \rightarrow$ ^{4}I$_{15/2}$ transition of Er^{3+}, can be well fitted related to the temperature, with the maximal S_A of 1.85% K^{-1} and 0.62% K^{-1} respectively. All the results suggest that LuVO$_4$: Yb^{3+}/Er^{3+} powders is a potential material for optical thermometry in both visible and NIR region based on FIR.

1. Introduction

Nowadays, the trivalent rare earth ions, such as Yb^{3+}/Er^{3+}, Yb^{3+}/Ho^{3+}, Yb^{3+}/Tm^{3+} etc., codoped UC luminescent materials have received widespread attention for their unique optical properties [1–3]. UC luminescence refers to the process of absorbing two or more low-energy photons and emitting one high-energy photon. Because of this, UC materials can convert the NIR light into the visible region. More importantly, UC materials have a large number of advantages over the organic dyes and quantum dots, such as narrow emission bandwidths, long luminescence lifetime, negligible autofluorescence background, high photostability and low toxicity [4–8]. The unparalleled physicochemical properties and stabilize optical properties make them more suitable to apply to

photonics, 3-D displays, optical encoding, bioimaging, etc. [9–11].

Moreover, for the UC luminescence materials, the potential application in temperature sensor has also been a hot research topic in recent years. Compared with traditional contact temperature sensing materials, optical temperature sensing materials have great advantages, such as non-contact, quick response, excellent precision and high accuracy [12,13]. In especial, the optical temperature sensors which depend on the FIR thermometry have been regarded as the promising temperature sensing materials, resulting from the strong anti-interference capacity.

Until now, most of the optical temperature sensing investigations based on FIR are focus on Yb^{3+} and Er^{3+} codoped UC materials. In Yb^{3+} and Er^{3+} codoped system, Yb^{3+} ions have large absorption cross-section at 980 nm. Furthermore, the ET processes from Yb^{3+} to Er^{3+} are very efficient. Therefore, a bright green UC emission of Er^{3+} can be detected, which is attributed to ^{2}H$_{11/2} \rightarrow$ ^{4}I$_{15/2}$ transition and ^{4}S$_{3/2} \rightarrow$ ^{4}I$_{15/2}$ transition. Fortunately, ^{2}H$_{11/2}$ energy level and ^{4}S$_{3/2}$ energy level are thermally coupled excited

states, which is very well suited for the studies of optical temperature sensing based on *FIR* [14].

Nevertheless, in order to obtain excellent precision and repeatability, intense UC emission is required. As is known to all, β-NaYF$_4$ and β-NaLuF$_4$ are the two most efficient hosts for UC, resulting from their low photon energy (~360 cm^{-1}) [15–18]. However, the low chemical stability of fluoride materials, especially in high temperature range, handicaps their utilization in thermometry. Therefore, the oxides, which possess extremely chemical stability as well as low photon energy, may be the suitable candidates. [28–30] For instance, Meng et al. and Carvajal et al. have demonstrated that YVO$_4$: Yb^{3+}/Er^{3+} and GdVO$_4$: Yb^{3+}/Er^{3+} are wonderful UC materials for luminescence temperature sensors based on *FIR* respectively [19,20]. As another important vanadate, LuVO$_4$, with the similar structure to YVO$_4$ and GdVO$_4$, is also an efficient matrix for UC. More importantly, the trivalent rare earth ions doped LuVO$_4$ phosphors may show stronger UC intensity than that of YVO$_4$ and GdVO$_4$ phosphors, which is due to the unique electronic state at the top of the valence of lutetium. This phenomenon has been proved in several isostructural materials, such as Y$_2$O$_3$ and Lu$_2$O$_3$, β-NaYF$_4$ and β-NaLuF$_4$, YF$_3$ and LuF$_3$ [17,31–33]. However, as far as we know, the paper concerning the temperature sensing properties in LuVO$_4$: Yb^{3+}/Er^{3+} is seldom published.

In the present work, the traditional high temperature solid state method were employed to prepare the Yb^{3+} and Er^{3+} codoped LuVO$_4$ phosphors. The ET mechanisms have been studied in detail by UC and NIR spectra as well as decay curves. Meanwhile, the temperature sensing behaviors in visible and NIR region based on *FIR* have also been explored. In visible region, the optical temperature sensing was studied via the *FIR* of the two thermally coupled energy levels $^2H_{11/2}$ and $^4S_{3/2}$ of Er^{3+}. In NIR region, the *FIR*s of the splitting peaks of Er^{3+} $^4I_{13/2} \rightarrow {}^4I_{15/2}$ transition were utilized in optical thermometry, As far as we know, there is very few paper concerning this phenomenon. All the results indicates that LuVO$_4$: Yb^{3+}/Er^{3+} powders is a potential temperature sensing material in both visible and NIR region under 980 nm wavelength excitation.

2. Experimental

2.1. Chemicals

Rare earth oxides of SpecPure grade (Lu$_2$O$_3$, Yb$_2$O$_3$, Er$_2$O$_3$, 99.99%) were purchased from Beijing Founde Star Science & Technology Co, Ltd. Analytical grade NH$_4$VO$_3$ was obtained from Chongqing Chuandong Chemical (Group) Co, Ltd. All of the chemical reagents were employed as starting materials without further purification.

2.2. Synthesis of LuVO$_4$: x mol%Yb^{3+}/y mol%Er^{3+} (x = 0, 1, 5, 10, 20, 30; y = 0, 0.1, 0.5, 1, 2, 3)

LuVO$_4$: x mol% Yb^{3+}/y mol% Er^{3+} powders were synthesized by traditional high temperature solid state method. Specifically as follows, 2 mmol Re$_2$O$_3$ (Lu$_2$O$_3$, Yb$_2$O$_3$ and Er$_2$O$_3$ in proportion) powders and 4 mmol NH$_4$VO$_3$ were weighed and mixed in an agate mortar. Next, the mixture were pulverized for 40 min. Then, place the powders to an alumina crucible which has a lid. The powders were firstly pre-sintered at 600 °C for 6 h followed by an intermediate grinding for 15 min to improve sample homogeneity and then sintering at 1200 °C for 6 h. Finally, the samples were obtained after being naturally cooled down to room temperature and pulverized into fine powders for measurements. All the reaction were in a box-type furnace with air atmosphere under the heating rate of 2 °C/min. The reaction equation can be expressed as following: Lu$_2$O$_3$ + 2NH$_4$VO$_3$ → 2LuVO$_4$ + 2NH$_3$↑ + H$_2$O↑.

2.3. Characterization

Powder X-ray diffraction (XRD) data were obtained by Cu Kα radiation (λ = 1.540 56 Å) on a Bruker D8 advance diffractometer over the angular range 10° ≤ 2θ ≤ 80°. The UC and NIR emission spectra were identified by an FLS920 spectrometer purchased from Edinburgh Instruments. The fluorescence lifetimes were measured by a Tektronix digital oscilloscope (TDS 3052) equipped with an optical parametric oscillator (OPO) as the excitation source. The lifetimes were calculated by integrating the area under the corresponding lifetime curves with the normalized initial intensity.

3. Results and discussion

3.1. Structure

Fig. 1 (a) and (b) show the XRD patterns of LuVO$_4$: x mol% Yb^{3+}/1 mol% Er^{3+} and LuVO$_4$: 20 mol% Yb^{3+}/y mol% Er^{3+} as well as the standard XRD data of LuVO$_4$ (JCPDS 17-0880). All the XRD diffraction peaks of the samples match well with the pure tetragonal phase LuVO$_4$. Moreover, no other phase is detected with the increasing Yb^{3+} or Er^{3+} concentration in the XRD patterns,
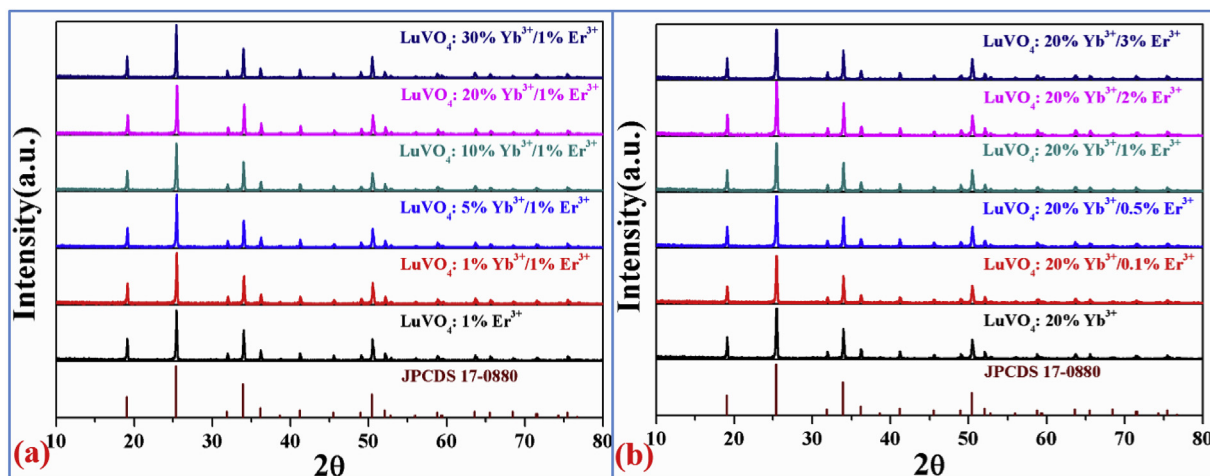

Fig. 1. The XRD patterns of LuVO$_4$: x mol%Yb^{3+}/y mol%Er^{3+} (x = 0, 1, 5, 10, 20, 30; y = 0, 0.1, 0.5, 1, 2, 3) with the standard XRD data of LuVO$_4$ (JCPDS 17-0880).
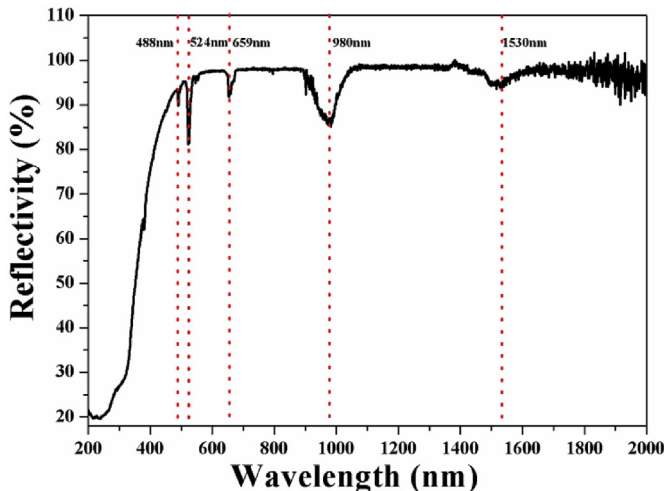
**Fig. 2.** The reflectance spectrum of LuVO$_4$: 20 mol% Yb^{3+}/2 mol% Er^{3+}.

demonstrating high concentration Yb^{3+} or Er^{3+} dopant has no effect on the crystal formation and transition, which is due to the similarity of ionic radius of Lu^{3+}, Yb^{3+} and Er^{3+}.

3.2. Luminescence properties

3.2.1. The reflectance spectrum of LuVO$_4$: Yb^{3+}/Er^{3+} powders

The reflectance spectrum of LuVO$_4$: 20 mol% Yb^{3+}/2 mol% Er^{3+} has been measured from 200 nm to 2000 nm, as shown in Fig. 2. There is a remarkable drop from 450 to 300 nm, which is due to the LuVO$_4$ host. Besides that, five distinct absorption peaks appear in the reflectance spectrum: Er^{3+}: $^4I_{15/2} \rightarrow {}^4F_{7/2}$ at 488 nm, Er^{3+}: $^4I_{15/2} \rightarrow {}^2H_{11/2}$ at 524 nm, Er^{3+}: $^4I_{15/2} \rightarrow {}^4F_{9/2}$ at 659 nm, Yb^{3+}: $^2F_{7/2} \rightarrow {}^2F_{5/2}$ at 980 nm and Er^{3+}: $^4I_{15/2} \rightarrow {}^4I_{13/2}$ at 1530 nm.

3.2.2. The UC properties of LuVO$_4$: Yb^{3+}/Er^{3+} powders

Fig. 3 (a) and (b) show the UC emission spectra of LuVO$_4$: x mol% Yb^{3+}/y mol% Er^{3+} powders under 980 nm wavelength excitation at low-output power density. Two strong green emission peaks and one weak red emission are observed in the range of 500 nm−700 nm. Since Yb^{3+} ions have only one excited level at approximately 980 nm, the three emission peaks all belong to Er^{3+} ions: $^2H_{11/2} \rightarrow {}^4I_{15/2}$ transition peaked at 524 nm, $^4S_{3/2} \rightarrow {}^4I_{15/2}$ transition peaked at 553 nm and $^4F_{9/2} \rightarrow {}^4I_{15/2}$ transition peaked at

659 nm. Moreover, as shown in Fig. 3 (a), with the increasing of Yb^{3+} doping concentration from 0 to 20 mol% accompanied by a fixed Er^{3+} doping concentration 1 mol%, the UC intensity is enhanced distinctly, which is an obvious evidence of ET from Yb^{3+} to Er^{3+}. However, when Yb^{3+} doping concentration is higher than 20 mol%, the UC intensities are decreased, resulting in the serious concentration quenching. That is to say, the optimal doping concentration of Yb^{3+} ions in LuVO$_4$ powders is 20 mol%. In addition, as presented in Fig. 3 (b), with the increasing of Er^{3+} doping concentration from 0 to 3 mol% accompanied by a fixed Yb^{3+} doping concentration 20 mol%, the UC emission intensity is enhanced dramatically and then decreased with Er^{3+} concentration above 2 mol%, which means that 2 mol% is the optimal doping concentration of Er^{3+} in this case. Consequently, the optimal composition for the strongest UC emission is considered to be LuVO$_4$: 20 mol % Yb^{3+}/2 mol % Er^{3+}.

Fig. 4 shows the NIR spectra of LuVO$_4$: 20 mol% Yb^{3+}/y mol% Er^{3+} powders under 980 nm wavelength excitation. Two strong emission bands appear in the range of 900 nm−1700 nm, which are assigned to Yb^{3+}: $^2F_{5/2} \rightarrow {}^2F_{7/2}$ transition and Er^{3+}: $^4I_{13/2} \rightarrow {}^4I_{15/2}$ transition respectively. Obviously, with the increasing of Er^{3+} doping concentration, $^2F_{5/2} \rightarrow {}^2F_{7/2}$ transition of Yb^{3+} is decreased dramatically, demonstrating the existence of ET from Yb^{3+} to Er^{3+}. Subsequently, the decay curves of $^2F_{5/2}$ energy level of Yb^{3+} are also measured and shown in Fig. 5. As can be seen clearly, the decay of Yb^{3+} $^2F_{5/2}$ level is greatly accelerated accompanying the increase of Er^{3+} concentration, by which the ET process between Yb^{3+} and Er^{3+} is further proved. Table 1 shows the lifetimes and ET efficiency (η_{ETE}) of Yb^{3+} $^2F_{5/2}$ level. The η_{ETE} is obtained as a function of Er^{3+} concentration: $\eta_{ETE,Er(x\%)} = 1 - \tau_{Er(x\%)}/\tau_0$, where $\tau_{Er(x\%)}$ represents for the decay time of Yb^{3+}: $^2F_{5/2}$ level with various Er^{3+} concentration. The maximal η_{ETE} is 39.3% with the Er^{3+} concentration 3 mol%.

In order to explore the number of photons involved in the population of $^2H_{11/2}$/$^4S_{3/2}$ level and $^4F_{9/2}$ level, the pump power dependence curve of Er^{3+} $^2H_{11/2}$/$^4S_{3/2} \rightarrow {}^4I_{15/2}$ transition and $^4F_{9/2} \rightarrow {}^4I_{15/2}$ transition in LuVO$_4$: 20 mol % Yb^{3+}/2 mol % Er^{3+} powder are measured. As shown in Fig. 6, in the low power region, the n value of $^2H_{11/2}$/$^4S_{3/2} \rightarrow {}^4I_{15/2}$ transition and $^4F_{9/2} \rightarrow {}^4I_{15/2}$ transition are 2 and 1.9 respectively, indicating both $^2H_{11/2}$/$^4S_{3/2} \rightarrow {}^4I_{15/2}$ transition and $^4F_{9/2} \rightarrow {}^4I_{15/2}$ transition are a two-photon process. However, in the high power region, the n value of $^2H_{11/2}$/$^4S_{3/2} \rightarrow {}^4I_{15/2}$ transition and $^4F_{9/2} \rightarrow {}^4I_{15/2}$ transition are all decreased, resulting from the competition between linear decay and UC processes for the deexcitation of the intermediate exited states which has been demonstrated by Pollnau's group [21]. The relevant ET
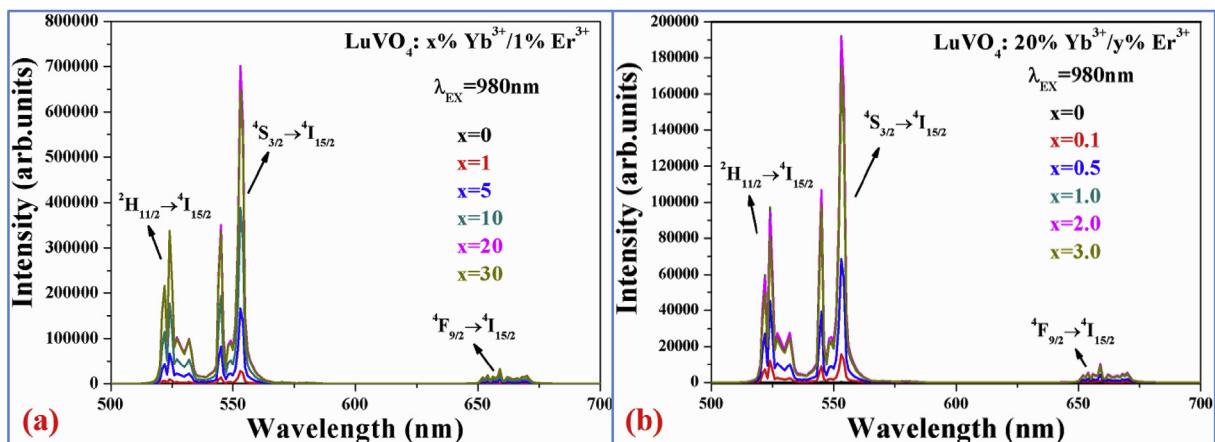

Fig. 3. Emission spectra of (a) LuVO$_4$: x mol% Yb^{3+}/1 mol% Er^{3+} powders (x = 0, 1, 5, 10, 20, 30) and (b) LuVO$_4$: 20 mol% Yb^{3+}/y mol% Er^{3+} powders (y = 0, 0.1, 0.5, 1.0, 2.0, 3.0) in visible region excited by 980 nm wavelength.
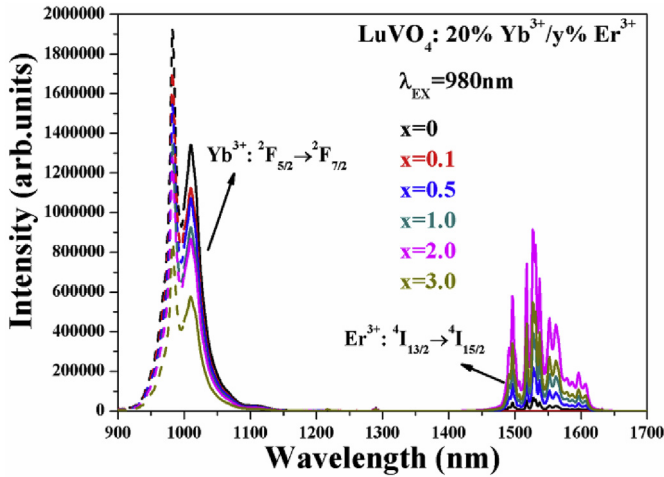
Fig. 4. Emission spectra of LuVO$_4$: 20 mol% Yb^{3+}/y mol% Er^{3+} powders ($y = 0$, 0.1, 0.5, 1.0, 2.0, 3.0) in NIR region under 980 nm wavelength excitation.

processes have been depicted in Fig. 7.

3.2.3. The temperature sensing properties of LuVO$_4$: Yb^{3+}/Er^{3+} powders

Fig. 8 shows the temperature dependence of UC emission from 303 K to 423 K excited by 980 nm wavelength at low power density. As can be seen clearly, the FIR of $^2H_{11/2} \rightarrow {}^4I_{15/2}$ transition to $^4S_{3/2} \rightarrow {}^4I_{15/2}$ transition is increased regularly with the rising temperature due to the thermal coupling between these two energy levels. According to the Boltzmann population distribution, the FIR of $^2H_{11/2} \rightarrow {}^4I_{15/2}$ transition to $^4S_{3/2} \rightarrow {}^4I_{15/2}$ transition can be expressed as:
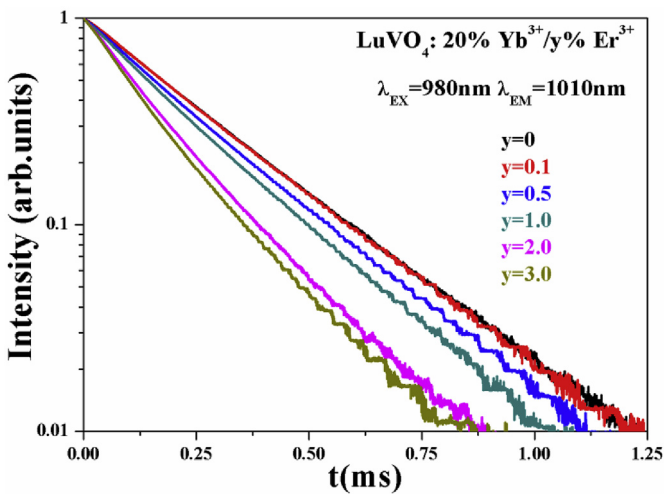
Fig. 5. Decay curves of $^2F_{5/2}$ energy level of Yb^{3+} in LuVO$_4$: 20 mol% Yb^{3+}/y mol% Er^{3+} powders under 980 nm wavelength excitation.

Table 1
The lifetimes and η_{ETE} of Yb^{3+} $^2F_{5/2}$ level in LuVO$_4$: 20 mol% Yb^{3+}/y mol% Er^{3+} powders.

Concentration of Er^{3+}(mol%)	Lifetime (μs)	η_{ETE}(%)
0	257.3	0
0.1	256.0	0.5
0.5	233.5	9.2
1.0	212.8	17.3
2.0	168.6	34.5
3.0	156.1	39.3
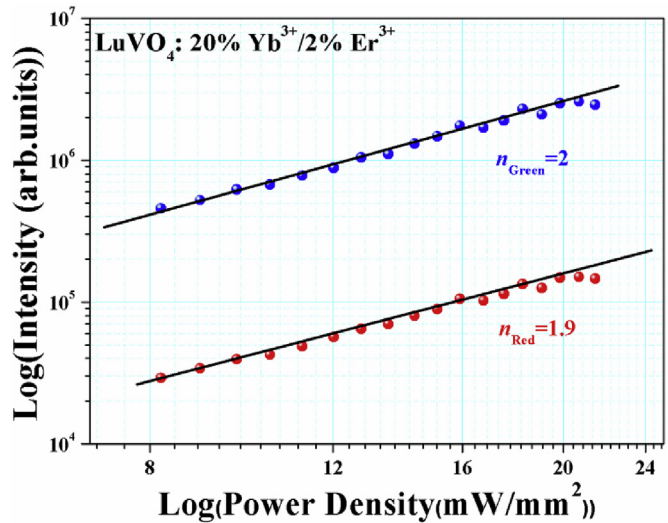
Fig. 6. Pump power dependence curve of Er^{3+} $^2H_{11/2}/^4S_{3/2} \rightarrow {}^4I_{15/2}$ transition and $^4F_{9/2} \rightarrow {}^4I_{15/2}$ transition in LuVO$_4$: 20 mol % Yb^{3+}/2 mol % Er^{3+} powder excited by 980 nm wavelength.

$$FIR = \frac{I_H}{I_S} = \frac{N_H \omega_H A_H}{N_S \omega_S A_S} e^{-\frac{\Delta E}{K_B T}} = B e^{-\frac{\Delta E}{K_B T}}, \tag{1}$$

where I represents for the UC intensity, N represents for the population of the energy level, w represents for the frequency, A represents for the non-radiative rate, g represents for the degeneracy degree, ΔE represents for the energy gap between $^2H_{11/2}$ and $^4S_{3/2}$, k_B represents for the Boltzmann constant, T represents for the absolute temperature, B represents for $g_H w_H A_H/g_S w_S A_S$ [18]. Based on equation (1), the temperature dependence curve of FIR can be fitted well as the following equation and is shown in Fig. 9 (a).

$$FIR = 16.14 e^{-1030/T} \tag{2}$$

The energy gap ΔE between $^2H_{11/2}$ level and $^4S_{3/2}$ level calculated by equation (2) is 716 cm^{-1}. The absolute sensitivity S_A and relative sensitivity S_R, which are the important information to assess the temperature sensing materials, can be written as
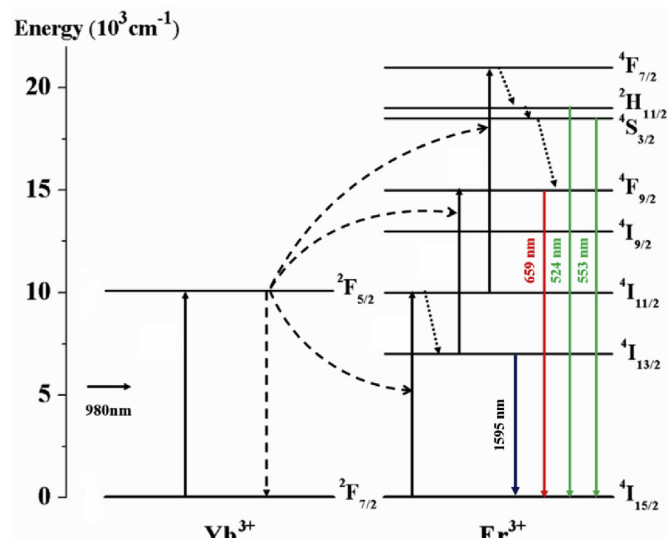

Fig. 7. The relevant ET processes in LuVO$_4$: 20 mol % Yb^{3+}/2 mol % Er^{3+} powder excited by 980 nm wavelength.
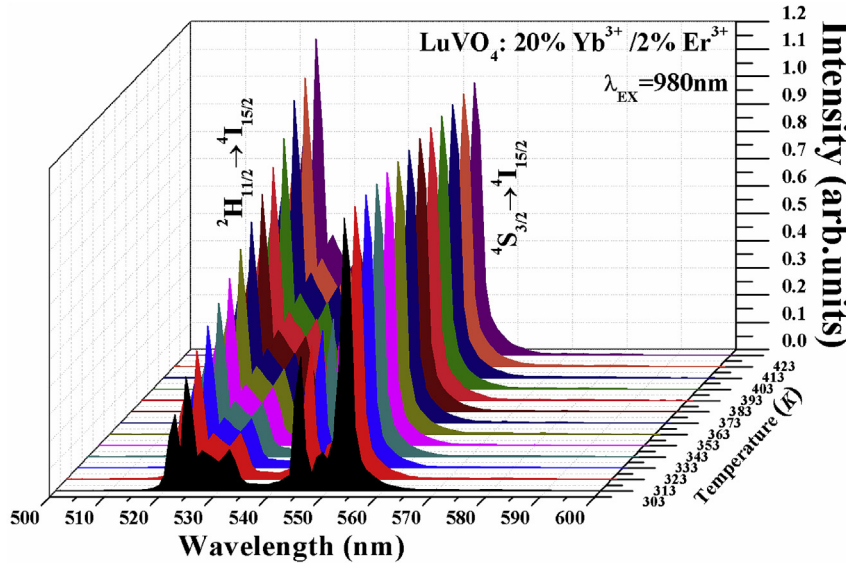
Fig. 8. The UC spectra of LuVO₄: 20 mol % Yb³⁺/2 mol % Er³⁺ powder excited by 980 nm wavelength at various temperatures from 303 K to 423 K. The intensities of $^4S_{3/2} \to {^4I_{15/2}}$ transition are normalized.

$$S_A = \left| \frac{d(FIR)}{dT} \right| = (FIR) \cdot \frac{\Delta E}{K_B T^2}, \tag{3}$$

$$S_R = \left| \frac{d(FIR)}{(FIR) \cdot dT} \right| = \frac{\Delta E}{K_B T^2}. \tag{4}$$

Since the values of S_A and S_R is proportional to ΔE, high S_A and S_R can be obtained in LuVO₄: Yb³⁺/Er³⁺ powder. Fig. 9 (b) depicts the temperature dependence of S_A and S_R in the range of 303 K–423 K.

Table 2
S_R of typical *FIR* temperature sensing materials on the basis of $^2H_{11/2} \to {^4I_{15/2}}$ transition and $^4S_{3/2} \to {^4I_{15/2}}$ transition of Er³⁺.

Sensing Materials	T (K)	S_R (%K⁻¹)	Reference
NaLuF₄: Yb³⁺/Er³⁺	295–343	1073/T²	[22]
LuVO₄: Yb³⁺/Er³⁺	303–423	1030/T²	This work
Y₀.₉₇₇Yb₀.₀₂Er₀.₀₀₃NbO₄:Yb³⁺/Er³⁺	300–573	1016/T²	[23]
BaMoO₄:Yb³⁺/Er³⁺	303–463	946/T²	[24]
NaGd(WO₄)₂:Yb³⁺/Er³⁺	293–573	895/T²	[25]
Y₂O₃:Er³⁺/Yb³⁺	93–643	886/T²	[26]
La₂O₃: Yb³⁺/Er³⁺	303–600	814/T²	[27]
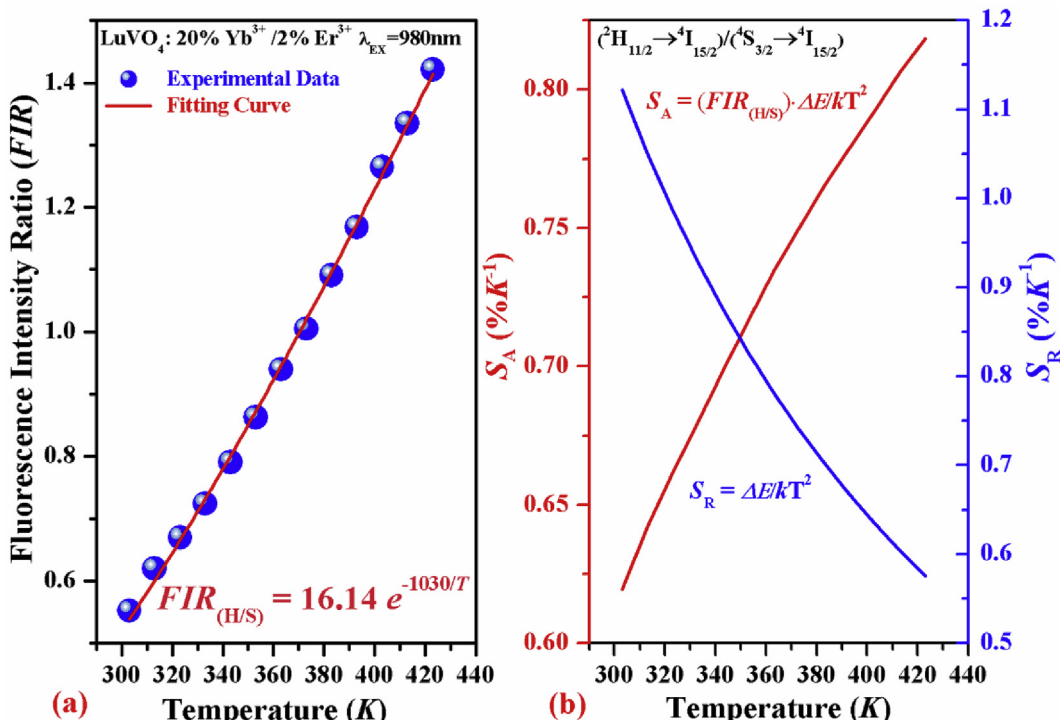
Fig. 9. Temperature dependence of (a) *FIR* between $^2H_{11/2} \to {^4I_{15/2}}$ transition and $^4S_{3/2} \to {^4I_{15/2}}$ transition of Er³⁺ and (b) absolute sensitivity S_A and relative sensitivity S_R in LuVO₄: 20 mol % Yb³⁺/2 mol % Er³⁺ powder.
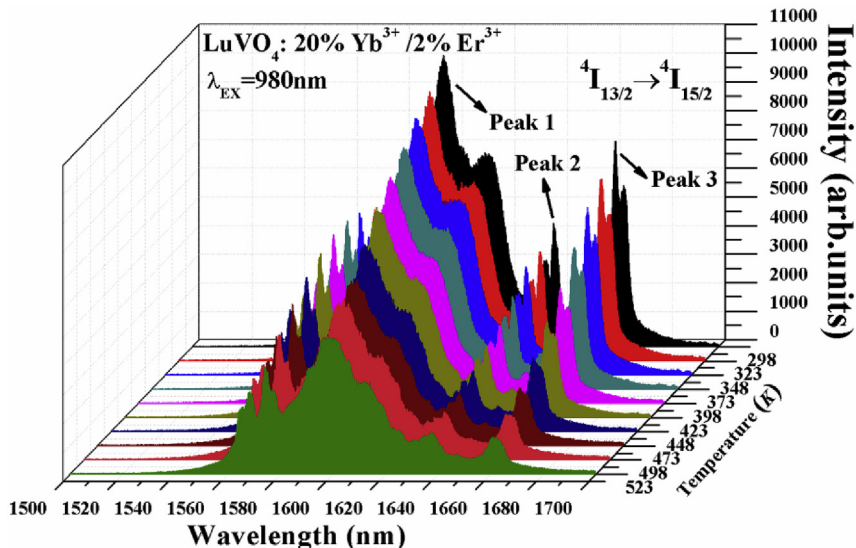
Fig. 10. Temperature dependence of $^4I_{13/2} \rightarrow {}^4I_{15/2}$ transition of Er^{3+} from 298 K to 523 K in LuVO$_4$: 20 mol % Yb^{3+}/2 mol % Er^{3+} powder under 980 nm wavelength excitation.

The S_A is increased accompanying the rising temperature and the maximum of S_A is 0.82% K^{-1} at 423 K. The S_R can be expressed as $1030/T^2$. Compared to a series of Yb^{3+} and Er^{3+} codoped temperature sensing materials (See Table 2), LuVO$_4$: Yb^{3+}/Er^{3+} sample displays an excellent sensitivity, demonstrating its potential application in temperature sensing.

Beyond that, under 980 nm wavelength excitation, the temperature dependence of $^4I_{13/2} \rightarrow {}^4I_{15/2}$ transition of Er^{3+} in LuVO$_4$: 20 mol % Yb^{3+}/2 mol % Er^{3+} powder is also investigated and shown in Fig. 10. The several peaks appearing in the range of 1500 nm−1700 nm all belong to $^4I_{13/2} \rightarrow {}^4I_{15/2}$ transition of Er^{3+}, due to the Stark splitting. The emission intensity is decreased distinctly with the rising temperature. More importantly, the *FIR*s of Peak 1 (located at 1595 nm) to Peak 3 (located at 1660 nm) and
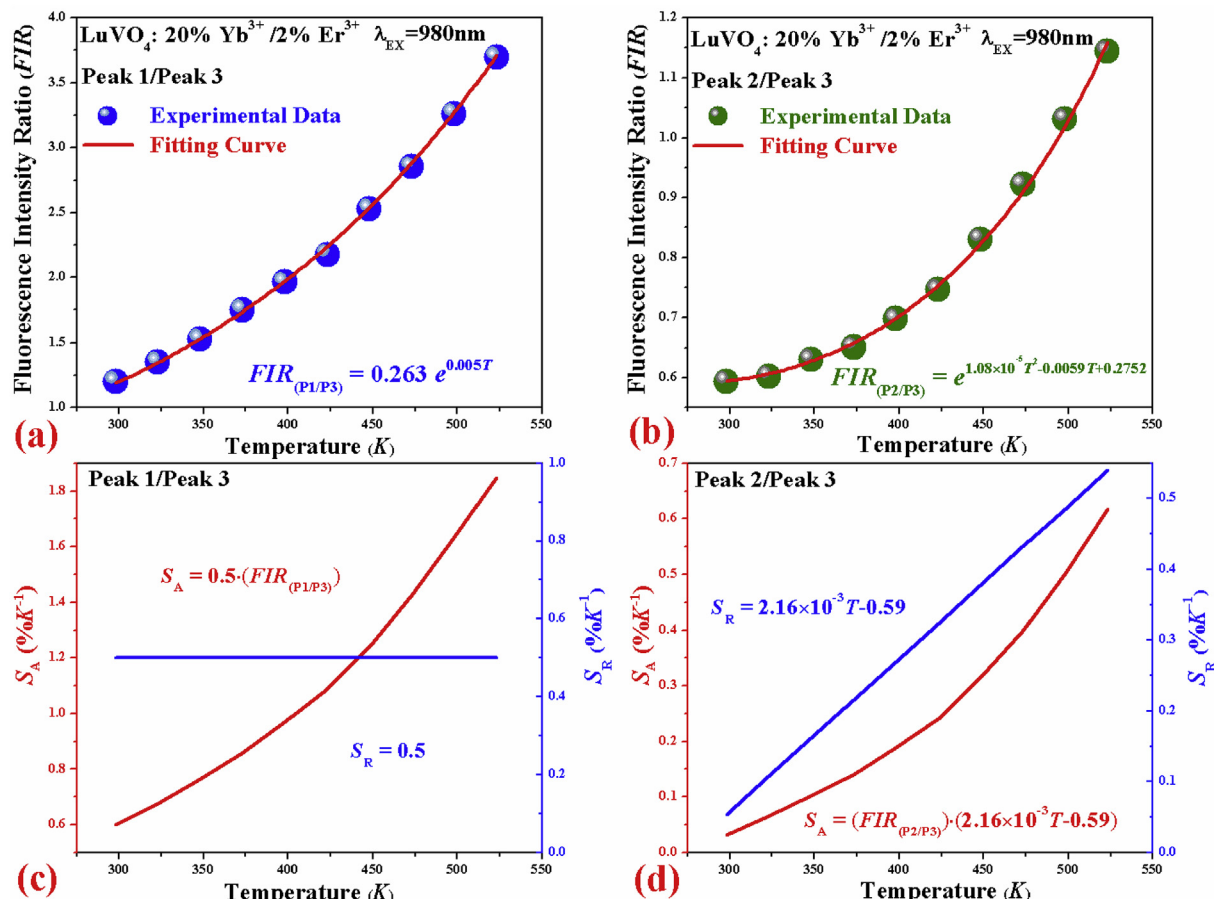

Fig. 11. Temperature dependence of *FIR* of (a) Peak 1 to Peak 3 and (b) Peak 2 to Peak 3; temperature dependence of S_A and S_R of (c) Peak 1 to Peak 3 and (d) Peak 2 to Peak 3.

Peak 2 (located at 1637 nm) to Peak 3 are changed regularly with the increasing temperature, as shown in Fig. 11 (a) and (b). The *FIR*s of Peak 1 to Peak 3 and Peak 2 to Peak 3 can be fitted well by the following equations respectively:

$$FIR_{(P1/P3)} = 0.263 \times e^{0.005T}, \tag{5}$$

$$FIR_{(P1/P3)} = e^{(1.08 \times 10-5 \ T2 - 0.005T + 0.2752)}. \tag{6}$$

The corresponding temperature dependence curves of S_A and S_R are also calculated and shown in Fig. 11 (c) and (d). Except for the S_R of Peak 1 to Peak 3 that keeps unchanged, the S_A of Peak 1 to Peak 3 and S_A and S_R of Peak 2 to Peak 3 are all increased with the rising temperature. The maximum of S_A of Peak 1 to Peak 3 is 1.85% K^{-1} at 523 K. The maximum of S_A and S_R of Peak 2 to Peak 3 is 0.62% K^{-1} and 0.53968% K^{-1} at 523 K respectively.

4. Conclusions

In summary, the LuVO$_4$: Yb^{3+}/Er^{3+} powders were synthesized by the traditional high temperature solid state method. The optimal doping concentration for Yb^{3+} and Er^{3+} is 20 mol % and 2 mol %, respectively. Thanks to the efficient ET processes from Yb^{3+} to Er^{3+} which have been demonstrated by the NIR spectra and lifetime curves, an intense green UC emission of Er^{3+} ^{2}H$_{11/2}$/^{4}S$_{3/2}$ → ^{4}I$_{15/2}$ transition can be observed under 980 nm wavelength excitation. Moreover, the LuVO$_4$: Yb^{3+}/Er^{3+} powders also have excellent performance on optical thermometry in visible region and NIR region. In visible region, based on the *FIR* of the two thermally coupled energy levels ^{2}H$_{11/2}$ and ^{4}S$_{3/2}$ of Er^{3+}, the maximum of S_A can be reached 0.82% K^{-1} at 423 K. In NIR region, the *FIR*s of Peak 1 (located at 1595 nm) to Peak 3 (located at 1660 nm) and Peak 2 (located at 1637 nm) to Peak 3, which are all attributed to ^{4}I$_{13/2}$ → ^{4}I$_{15/2}$ transition of Er^{3+}, can be well fitted related to the temperature, with the maximal absolute sensitivity S_A of 1.85% K^{-1} and 0.62% K^{-1} respectively. The results reveal that LuVO$_4$: Yb^{3+}/Er^{3+} powders is a promising temperature sensing material in both visible and NIR region under 980 nm wavelength excitation.

Acknowledgements

References

[1] J.H. Zhang, Z.D. Hao, J. Li, X. Zhang, Y.S. Luo, G.H. Pan, Light Sci. Appl. 4 (2015) e239.

[2] W.F. Rao, Q.S. Zhu, Q. Ren, C.C. Wu, J.H. Miao, Hydrothermal synthesis and up-conversion luminescence of Yb^{3+}/Ho^{3+} Co-doped Y$_6$WO$_{12}$ nanocrystals, J. Electron. Mater. 46 (2017) 5303–5307.

[3] Q. Liu, W. Zhang, Z.F. Hu, Z.Y. Feng, L. Ma, X.P. Zhang, X. Sheng, J. Luo, Improved near-infrared up-conversion emission of YAG: Yb, Tm phosphor substituted by gallium and indium, J. Mater. Sci. Mater. Electron. 27 (2016) 992–997.

[4] Y.N. Huang, Q.B. Xiao, H.S. Hu, K.C. Zhang, Y.M. Feng, F.J. Li, J. Wang, X.G. Ding, J. Jiang, Y.F. Li, L.Y. Shi, H.Z. Lin, 915 nm light-triggered photodynamic therapy and MR/CT dual-modal imaging of tumor based on the nonstoichiometric Na$_{0.52}$YbF$_{3.52}$: Er upconversion nanoprobes, Small 12 (2016) 4200–4210.

[5] H. Dong, L.D. Sun, Y.F. Wang, J. Ke, R. Si, J.W. Xiao, G.M. Lyu, S. Shi, C.H. Yan, Efficient tailoring of upconversion selectivity by engineering local structure of lanthanides in Na$_x$REF$_{3+x}$ nanocrystals, J. Am. Chem. Soc. 137 (2015) 6569–6576.

[6] M. Haase, H. Schäfer, Upconverting nanoparticles, Angew. Chem. Int. Ed. 50 (2011) 5808–5829.

[7] Q. Liu, Y. Sun, T.S. Yang, W. Feng, C.G. Li, F.Y. Li, Sub-10 nm hexagonal lanthanide-doped NaLuF$_4$ upconversion nanocrystals for sensitive bioimaging in vivo, J. Am. Chem. Soc. 133 (2011) 17122–17125.

[8] S.S. Cui, H.Y. Chen, H.Y. Zhu, J.M. Tian, X.M. Chi, Z.Y. Qian, S. Achilefu, Y.Q. Gu, Amphiphilic chitosan modified upconversion nanoparticles for in vivo photodynamic therapy induced by near-infrared light, J. Mater. Chem. 22 (2012) 4861–4873.

[9] W. Zheng, P. Huang, D.T. Tu, E. Ma, H.M. Zhu, X.Y. Chen, Lanthanide-doped upconversion nano-bioprobes: electronic structures, optical properties, and biodetection, Chem. Soc. Rev. 44 (2015) 1379–1415.

[10] J. Wang, T. Wei, X.Y. Li, B.H. Zhang, J.X. Wang, H. Huang, Q. Yuan, Near-infrared-light-mediated imaging of latent fingerprints based on molecular recognition, Angew. Chem. 126 (2014) 1642–1646.

[11] C.X. Li, D.M. Yang, P.A. Ma, Y.Y. Chen, Y. Wu, Z.Y. Hou, Y.L. Dai, J.H. Zhao, C.P. Sui, J. Lin, Multifunctional upconversion mesoporous silica nanostructures for dual modal imaging and in vivo drug delivery, Small 9 (2013) 4150–4159.

[12] C.D.S. Brites, P.P. Lima, N.J.O. Silva, A. Millan, V.S. Amaral, F. Palacio, L.D. Carlos, Thermometry at the nanoscale, Nanoscale 4 (2012) 4799–4829.

[13] D. Jaque, F. Vetrone, Luminescence nanothermometry, Nanoscale 4 (2012) 4301–4326.

[14] X. Wang, Q. Liu, Y. Bu, et al., Optical temperature sensing of rare-earth ion doped phosphors, RSC Adv. 5 (2015) 86219–86236.

[15] Y. Wei, F.Q. Lu, X.R. Zhang, D.P. Chen, Synthesis of oil-dispersible hexagonal-phase and hexagonal-shaped NaYF$_4$: Yb, Er nanoplates, Chem. Mater. 18 (2006) 5733–5737.

[16] Y. Li, X. Cao, G.F. Wang, S. Liu, L. Feng, B.,Y. Xu, Y.,P. Wang, J.M. Su, Synthesis and tunable upconversion luminescence of NaLuF$_4$: Yb^{3+}/Er^{3+} nanocrystals by Pb^{2+} tridoping, Sci. Adv. Mater. 6 (2014) 1037–1042.

[17] E.J. He, H.R. Zheng, W. Gao, Y.X. Tu, Y. Lu, G.A. Li, Investigation of upconversion and downconversion fluorescence emissions from β-NaLn1F$_4$:Yb^{3+}, Ln2^{3+} (Ln1 = Y, Lu; Ln2 = Er, Ho, Tm, Eu) hexagonal disk system, Mater. Res. Bull. 48 (2013) 3505–3512.

[18] S. Jiang, P. Zeng, L.Q. Liao, S.F. Tian, H. Guo, Y.H. Chen, C.K. Duan, M. Yin, Optical thermometry based on upconverted luminescence in transparent glass ceramics containing NaYF$_4$: Yb^{3+}/Er^{3+}, nanocrystals, J. Alloys Compd. 617 (2014) 538–541.

[19] A.S. Oleksandr, J.C. Joan, C. Cascales, M. Aguiló, F. Díaz, Benefits of silica Core–Shell structures on the temperature sensing properties of Er,Yb:GdVO$_4$ up-conversion nanoparticles, ACS Appl. Mater. Interfaces 8 (2016) 7266–7273.

[20] Q.Y. Meng, T. Liu, J.Q. Dai, W.J. Sun, Study on optical temperature sensing properties of YVO$_4$:Er^{3+}, Yb^{3+} nanocrystals, J. Lumin. 179 (2016) 633–638.

[21] M. Pollnau, D.R. Gamelin, S.R. Lüthi, H.U. Güdel, Power dependence of upconversion luminescence in lanthanide and transition-metal-ion systems, Phys. Rev. B 61 (2000) 3337–3346.

[22] D.Y. Li, L. Tian, Z. Huang, L.X. Shao, J. Quan, Y.X. Wang, Optical temperature sensor based on infrared excited green upconversion emission in hexagonal phase NaLuF$_4$:Yb^{3+}/Er^{3+} nanorods, J. Nanosci. Nanotechnol. 16 (2016) 3641–3645.

[23] A.K. Singh, S.K. Singh, B.K. Gupta, R. Prakash, S.B. Rai, Probing a highly efficient dual mode: down-upconversion luminescence and temperature sensing performance of rare-earth oxide phosphors, Dalton Trans. 42 (2013) 1065–1072.

[24] A.K. Soni, A. Kumari, V.K. Rai, Optical investigation in shuttle like BaMoO$_4$: Er^{3+}-Yb^{3+} phosphor in display and temperature sensing, Sens. Actuators, B 216 (2015) 64–71.

[25] J.S. Liao, L. Nie, Q. Wang, S.J. Liu, H.R. Wen, J.P. Wu, NaGd(WO$_4$)$_2$:Yb^{3+}/Er^{3+} phosphors: hydrothermal synthesis, optical spectroscopy and green upconverted temperature sensing behavior, RSC Adv. 6 (2016) 35152–35159.

[26] P. Du, L.H. Luo, Q.Y. Yue, W.P. Li, The simultaneous realization of high- and low-temperature thermometry in Er^{3+}/Yb^{3+} -codoped Y$_2$O$_3$. nanoparticles, Mater. Lett. 143 (2015) 209–211.

[27] R. Dey, V.K. Rai, Yb^{3+} sensitized Er^{3+} doped La$_2$O$_3$ phosphor in temperature sensors and display devices, Dalton Trans. 43 (2013) 111–118.

[28] V.G. Tamara, J.J. Dragana, S. Krisjanis, D.D. Miroslav, Multicolor upconversion luminescence of GdVO4:ln^{3+}/Yb^{3+} (Ln^{3+} = Ho^{3+}, Er^{3+}, Tm^{3+}, Ho^{3+}/Er^{3+}/Tm^{3+}) nanorods, Dyes Pigments 126 (2016) 1–7.

[29] V.G. Tamara, J.J. Dragana, L. Vesna, D.D. Miroslav, Multifunctional Eu^{3+}-and Er^{3+}/Yb^{3+}-doped GdVO$_4$ nanoparticles synthesized by reverse micelle method, Sci. Rep. 4 (2014) 4209.

[30] M. Venkataramanan, N. Rafik, V. Fiorenzo, A.C. John, Enhancing upconverted white light in Tm^{3+}/Yb^{3+}/Ho^{3+}-doped GdVO$_4$ nanocrystals via incorporation of Li$^+$ ions, Opt. Exp. 20 (2012) 111–119.

[31] Y.P. Li, J.H. Zhang, X. Zhang, Y.S. Luo, X.G. Ren, H.F. Zhao, X.J. Wang, L.D. Sun, C.H. Yan, Near-infrared to visible upconversion in Er^{3+} and Yb^{3+} codoped Lu$_2$O$_3$ nanocrystals: enhanced red color upconversion and three-photon process in green color upconversion, J. Phys. Chem. C 113 (2009) 4413–4418.

[32] J.A. Capobianco, F. Vetrone, J.C. Boyer, A. Speghini, M. Bettinelli, Visible upconversion of Er^{3+} doped nanocrystalline and bulk Lu$_2$O$_3$, Opt. Mater. 19 (2002) 259–268.

[33] G.T. Xiang, J.H. Zhang, Z.D. Hao, X. Zhang, G.H. Pan, L. Chen, Y.S. Luo, S.Z. Lü, H.F. Zhao, Solvothermal synthesis and upconversion properties of about 10 nm orthorhombic LuF$_3$: Yb^{3+}, Er^{3+} rectangular nanocrystals, J. Colloid Interface Sci. 459 (2015) 224–229.